

IM-IAD: Industrial Image Anomaly Detection Benchmark in Manufacturing

Guoyang Xie¹, Jinbao Wang¹, Jiaqi Liu¹, Jiayi Lyu, Yong Liu, Chengjie Wang, Feng Zheng, *Member, IEEE*, and Yaochu Jin, *Fellow, IEEE*

Abstract—Image anomaly detection (IAD) is an emerging and vital computer vision task in industrial manufacturing (IM). Recently many advanced algorithms have been published, but their performance deviates greatly. We realize that the lack of actual IM settings most probably hinders the development and usage of these methods in real-world applications. As far as we know, IAD methods are not evaluated systematically. As a result, this makes it difficult for researchers to analyze them because they are designed for different or special cases. To solve this problem, we first propose a uniform IM setting to assess how well these algorithms perform, which includes several aspects, i.e., various levels of supervision (unsupervised vs. semi-supervised), few-shot learning, continual learning, noisy labels, memory usage, and inference speed. Moreover, we skillfully build a comprehensive image anomaly detection benchmark (IM-IAD) that includes 16 algorithms on 7 mainstream datasets with uniform settings. Our extensive experiments (17,017 in total) provide in-depth insights for IAD algorithm redesign or selection under the IM setting. Next, the proposed benchmark IM-IAD gives challenges as well as directions for the future. To foster reproducibility and accessibility, the source code of IM-IAD is uploaded on the website, <https://github.com/M-3LAB/IM-IAD>.

I. INTRODUCTION

There is a strong need to propose a uniform industrial highly relevant setting to tap the gap, which brings the IAD algorithm’s capabilities into the factory floor. Image anomaly detection (IAD) is an important computer vision task for industrial manufacturing applications like battery surface anomaly detection [68], ceramic defect detection [37], food inspection [69], and so on. Due to the gap between academia and industrial manufacturing, only a few IAD algorithms are used in real manufacturing. In the computer vision community, there is a primary focus on unsupervised methods, but there is little analysis of the industry’s demands. Because of this, it is important and urgent to build a uniform setting for industrial

Guoyang Xie is with the Department of Computer Science and Engineering, Southern University of Science and Technology, Shenzhen 518055, China and is also with the Department of Computer Science, University of Surrey, Guildford GU2 7YX, United Kingdom (e-mail: guoyang.xie@surrey.ac.uk)

Jinbao Wang, Jiaqi Liu and Feng Zheng are with the Department of Computer Science and Engineering, Southern University of Science and Technology, Shenzhen 518055, China (e-mail: linkingring@163.com; liujq32021@mail.sustech.edu.cn; f.zheng@ieee.org)

Yong Liu and Chengjie Wang are with Tencent Youtu Lab, Shenzhen 518040, China (e-mail: chaosliu@tencent.com; jasoncjwang@tencent.com)

Jiayi Lyu is with the School of Engineering Science, University of Chinese Academy of Sciences, Beijing, China (e-mail: lyujiayi21@mailsucas.ac.cn)

Yaochu Jin is with the Faculty of Technology, Bielefeld University, 33619 Bielefeld, Germany and also with the Department of Computer Science and Engineering, University of Surrey, Guildford GU2 7YX, United Kingdom (e-mail: yaochu.jin@uni-bielefeld.de)

¹Contributed Equally.

TABLE I

THE COMPARISON WITH IAD AND THE EXISTING RELATED BENCHMARKS IN TERMS OF DATASET, LEARNING PARADIGM, ALGORITHM AND METRIC.

Work		[83]	[24]	IM-IAD	
Dataset	MVTec AD	✓	✓	✓	
	MVTec LOCO-AD			✓	
	BTAD			✓	
	MPDD			✓	
	MTD			✓	
	VisA			✓	
	DAGM			✓	
Paradigm	Supervision		✓	✓	
	Noisy		✓	✓	
	Few-Shot			✓	
	Continual			✓	
	Uniform			✓	
Algorithm	Feature Embedding	Normalizing Flow	✓	✓	
		Memory Bank	✓	✓	
		Teacher-Student	✓	✓	
	Reconstruction	One-Class Classification	✓		✓
		External Data	✓		✓
		Internal Data	✓		✓
Metric	AUROC	Image-Level	✓	✓	
		Pixel-Level	✓	✓	
	AP	Image-Level	✓		✓
		Pixel-Level	✓		✓
PRO				✓	
SPRO				✓	
FM				✓	
Efficiency	Inference Speed	✓		✓	

manufacturing that can adapt IAD algorithms to the needs of industrial manufacturing.

Uniform IM setting is more capable to assess IAD performance in real-world industrial manufacturing. Uniform IM setting contains few-shot, semi-supervised, continual learning and noisy labeling. Previous works have achieved some progress in one of uniform IM setting, like DRA [22], Softpach [71] and DRE [39]. However, their proposed solution can not meet the full requirements of industrial manufacturing. For instance, semi-supervised IAD setting [48] assumes that the training dataset consists of a large number of normal samples and limited abnormal samples. However, it is difficult to achieve numerous normal samples due to the high defection rate during manufacturing changeover, violating the assumption of semi-supervised IAD setting. As for changeover scenarios, the few-shot setting proposed by GraphCore [1] is more suitable to outline the challenges. Therefore, our uniform IM setting is pushing cutting-edge IAD methods to meet the demands of industrial manufacturing.

Regarding our uniform IM setting, the following is a summary of the challenging issues that need to be simultaneously investigated:

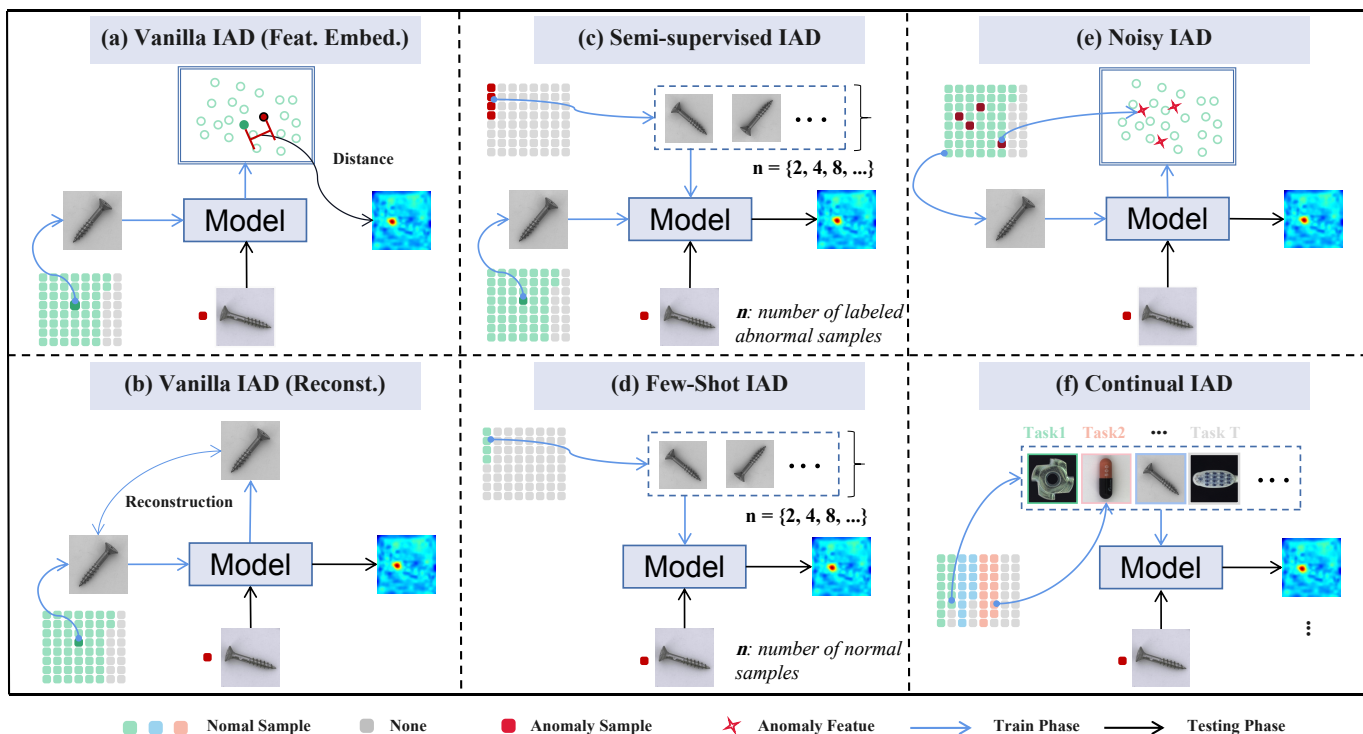


Fig. 1. Vanilla unsupervised IAD methods can be divided into two categories, namely feature embedding and reconstruction-based method. As shown in (a), feature embedding methods compare the difference between test samples and normal samples at the feature level, while reconstruction-based methods compare the difference between the input image and the reconstructed image to determine whether it is abnormal or not, as shown in (b). For semi-supervised methods as shown in (c), they use limited abnormal samples with annotations to improve model performance. The few-shot setting (d) only utilizes a small number of normal samples for training. The noisy setting (e) mixes abnormal samples in the training set and evaluates the robustness of the model. The continual setting (f) trains on each task in turn and evaluates how much the model forgets past tasks. The details of IM setting are described in Sec. III-A.

1) The remaining challenges for semi-supervised IAD [22], [43] described in Fig. 1(c) is how to effectively utilize the guidance from limited abnormal data and a large number of normal samples to detect the anomalies.

2) For few-shot IAD presented in Fig. 1(d), we attempt to detect anomalies in the test dataset using a small number of normal or abnormal images as the training dataset [1]. The major obstacles are i) In an unsupervised setting, the training dataset for each category contains only normal samples, meaning that there are no annotations at the image or pixel level. ii) In an unsupervised setting, few normal samples of the training set are accessible. In the setting we propose, there are fewer than eight training samples.

3) We attempt to detect the abnormal sample and identify anomalies given a target category for IAD in the presence of noise [71] described in Fig. 1(e). However, the training dataset contains a significant amount of noisy data, *i.e.* label flipping. Since the anomalies are too tiny to identify, abnormal samples are easily mislabeled as normal ones. The most significant barrier are i) Each category's training dataset contains noisy data that could easily confuse the decision threshold of IAD algorithms. ii) There are a large number of noisy data. In our proposed situation, the percentage of anomalous samples in the training set ranges from 5% to 20%.

4) For the continual IAD presented in Fig. 1(f), the most significant barrier is that IAD algorithms may suffer from catastrophic forgetting when they have completed training on

the new category dataset.

Previous IAD benchmarks cannot accurately reflect the needs of industrial manufacturing. There are two notable works [83], [24] that take effort to benchmark IAD algorithms. The distinction between IM-IAD and previous benchmarks lies in the following aspects: Firstly, previous studies mainly concentrate on benchmarking IAD methods based on the level of supervision [24]. However, they [83], [24] ignore the realistic scenarios of industrial manufacturing, *i.e.*, continual learning, changeover-based few-shot learning, and noisy labels. It is crucial because most IAD algorithms are unsuitable for production lines. Our proposed IM setting makes researchers aware of the gap between academia and industry and offers deeper insights into future improvements. Secondly, ADBench [24] focuses primarily on tabular and graph-structured data but not image data, and no IAD algorithms have been evaluated on the benchmark. Even for [83], they only assess unsupervised IAD algorithms on two datasets, which are not effective to rigorously assess IAD algorithms. However, we construct IM-IAD with 7 industrial datasets and 16 algorithms. We strive to address the above issues in IAD and illustrate the main differences in Table I.

Key Takeaways: Through extensive experiments, we find i) Regarding accuracy, memory usage and inference speed, none of the benchmarked unsupervised IAD algorithms is statistically better than others, emphasizing the importance of anomaly type selection. ii) Long-distance attention mech-

anism shows great potential in logical anomaly detection, possibly due to their global feature extraction abilities. iii) most unsupervised IAD methods can outperform the best semi-supervised IAD methods, justifying the efficiency of labelled anomalies usage. iv) with merely 4 augmented (rotated) data, feature embedding-based few-shot IAD algorithms can achieve 95% performance of vanilla IAD, revealing the necessity of data characteristics. v) Importance re-weighting successfully enhance the resilience of IAD algorithms even though the noise ratio is larger than 10%. vi) Memory bank can be seamlessly incorporated into cutting-edge IAD algorithms, considerably enhancing their capacity to resist catastrophic forgetting.

Overall, our contributions are summarized as follows:

- We extract scientific problems from the manufacturing process and present a standardized and unified setting to bridge the gap between academic research and industrial practices in the identification of image anomalies.
- We examine 16 image anomaly detection methods on 7 benchmark datasets, resulting in a total of 17,017 instances. Moreover, we present a plug-and-play and modular implementation for fair IAD evaluation, which greatly benefits the future development of IAD algorithms.
- By analyzing the requirements of research and industrial manufacturing processes, we examine four key aspects of IAD algorithms for comparison: the changeover-based few-shot representational abilities; the trade-off between accuracy and efficiency; the catastrophic forgetting phenomenon; and the robustness of the algorithm in the presence of noise labelling. Based on these aspects, we offer deep insights and suggest future directions.

II. RELATED WORK

A. Unsupervised IAD

There are two mainstreams of research on unsupervised industrial IAD, namely feature embedding-based methods [5], [55], [12], and reconstruction-based methods [75], [79].

1) *Feature embedding-based methods*: Specifically, feature embedding-based approaches can be divided into four categories, including teacher-student [5], normalizing flow [55], memory bank [12], and one-class classification [62]. We will explain these architectures in detail as follows.

Teacher-Student. Teacher-student model is one of the typical methods for industrial manufacturing IAD, such as [5], [57]. In the training phase, the teacher model extracts the features of normal samples and distills the knowledge to the student model. The parameters of the teacher model are frozen. In the test phase, the features of normal images extracted by the teacher network are similar to the ones extracted by the student network. Regarding the abnormal images, the features extracted by the teacher network may deviate from the ones from the student network. Thus, the feature difference in the teacher-student network is the most important principle in detecting anomalies. STPM [67] detects anomalies by multiplying the anomaly maps at three different resolutions. But, if one of the anomaly maps fails to detect an anomaly location, the anomaly

detection fails. For ameliorating the failure case of STPM, RSTPM [72] employs one more pair of the teacher-student network and the extra discriminate network, which enhances the ability of normal feature reconstruction and makes the normal features different from the abnormal features. However, the performance of anomaly detection heavily depends on the power of the teacher network, which may limit the ability of generalization.

Normalizing Flow (NF). NF [52] is a method for constructing complex distributions via transforming a probability density through a series of invertible mappings. In the training phase, NF IAD methods [78], [55] collect features from normal images from a pre-trained model, such as ResNet [25] or Swin Transformer [42], and convert the feature distribution into a Gaussian distribution. In the test phase, the features of abnormal images after passing through NF will deviate from the Gaussian distribution of the training phase, which is the most fundamental assumption to classify anomalies. As for enhancing the defect detection ability, CS-Flow [56] incorporates cross-convolution blocks into NF and uses a multi-scale feature map to identify anomalies. CFlow-AD [23] implements positional encoding inside the conditional NF to enhance performance. Nevertheless, the images from industrial manufacturing may contradict the strong assumption of NF. In other words, the features of normal images in industrial manufacturing may not adhere to Gaussian distributions, which may degrade anomaly detection performance.

Memory Bank. Memory bank-based methods for industrial IAD are simple but effective, such as [12], [38], [34]. In the training phase, memory bank-based approaches capture the features of normal images and store them in a feature memory bank. During the testing phase, the feature of the test sample queries the memory bank for the feature points of k-nearest neighborhoods. If the distance between the test feature and the closest feature points of neighbourhoods exceeds a specific threshold, the test sample is categorized as anomalous. SPADE [12] enhances the effectiveness of feature extraction by gathering multi-resolution features of pyramid architecture. To limit the size of the memory bank, PaDim [17] produces a probabilistic feature representation for all training images. Consequently, the size of the memory bank is closely correlated with image resolution but not with the size of the dataset. Nevertheless, the performance of anomaly detection heavily depends on the size of the memory bank. Hence, there are still several opportunities to investigate the trade-off between the algorithm's performance and the size of the memory bank.

One-Class Classification (OCC). Since anomaly detection aims to categorize the test sample as normal or abnormal, the issue can be recast as OCC [62], [45]. During training, OCC methods [76], [28] attempt to construct a hypersphere to separate the features of normal samples from the ones of abnormal samples. During inference, the method identifies whether the test sample is anomalous or not based on the location of the sample's features inside the hypersphere. PatchSVDD [76] splits all input images into patches of the same size for fine-grained anomaly detection. DSPSVDD [82] simultaneously minimizes the hypersphere volume and network reconstruction error for more effective feature extraction. SE-SVDD [28] pro-

poses a semantic correlation module to enhance the semantic representation ability of abnormal samples. The majority of OCC methods generate anomaly samples via data augmentation. But the low quality of synthesized abnormal samples will have a negative impact on the performance of anomaly detection.

2) *Reconstruction-based methods*: Reconstruction-based methods are relatively uniform, unlike the high diversity of feature embedding-based methods. A reconstruction network is often trained in a self-supervised manner, and the reconstruction network can restore various images to normal representations. After reconstruction, comparing the reconstructed image with the original image and the abnormal area will be significantly different between the two images. Although ideas are similar, some of them [79], [32], [81] rely on external datasets to generate anomalies to further enhance model generalization, while others [19], [80], [59] do not.

B. Semi-supervised IAD

Regarding the data setting, the distinction between unsupervised IAD and semi-supervised IAD [11], [65] is the use of abnormal images for training. Semi-supervised IAD methods [65], [48] focus on how to efficiently employ a small number of abnormal samples to distinguish the features of abnormalities from those of normal samples. Chu *et al.* [11] utilize the change in the loss function value to identify abnormal data. They train a neural batch sampler using a reinforcement learning algorithm to accentuate the difference in loss curves between anomalous and non-anomalous regions. DevNet [48] treats normal samples as a priori knowledge and proposes a multi-instance loss function to distinguish normal and abnormal samples in the feature-embedding space. Wang *et al.* [66] design a logit loss to mitigate the adverse impact of long-tail data distribution. In addition, they design an abnormality-capturing module for characterizing anomalous features. Nevertheless, the performance of semi-supervised visual anomaly detection approaches is inferior to that of unsupervised methods for identifying anomalies. There is still considerable room for improvement regarding the use of data from abnormal samples.

C. Few-shot IAD

Few-shot anomaly detection (FSAD) for IAD [70], [33] is still in its infancy. There are two settings in FSAD. The first setting is meta-learning [29]. In other words, this setting requires a large number of images as a meta-training dataset. Wu *et al.* [70] propose a novel architecture, called MetaFormer, that employs meta-learned parameters to achieve high model adaptation capability and instance-aware attention to localize abnormal regions. RegAD [29] trains a model for detecting category-agnostic anomalies. In the test phase, the anomalies are identified by comparing the registered features of the test image and its corresponding normal images. The second setting relies on vanilla few-shot image learning. PatchCore [54], SPADE [12], PaDim [18] conduct the ablation study on 16 normal training samples. None of them, however, are specialized in few-shot anomaly detection. Hence, it is

necessary to develop new algorithms that concentrate on native few-shot anomaly detection tasks.

D. Noisy IAD

Noisy learning is a classical problem for anomaly detection. Tan *et al.* [64] employ a novel trust region memory update scheme to keep noise feature points away from the memory bank. Yoon *et al.* [77] use a data refinement approach to improve the robustness of the one-class classification model. Qiu *et al.* [50] propose a strategy for training an anomaly detector in the presence of unlabeled anomalies, which is compatible with a broad class of models. They create labelled anomalies synthetically and jointly optimize the loss function with normal data and synthesis abnormal data. Chen *et al.* [9] introduce an interpolated Gaussian descriptor that learns a one-class Gaussian anomaly classifier trained with adversarially interpolated training samples. However, the majority of the aforementioned approaches have not been verified on real industrial image datasets. In other words, the effectiveness of the existing anomaly detection methods may not be suitable for industrial manufacturing.

III. IM-IAD

The inference goal is identical for the few-shot IAD and noisy IAD settings, *i.e.*, given a normal or abnormal sample from a target category, the anomaly detection model should predict whether or not the image is anomalous and localize the anomaly region if the prediction result is anomalous.

A. Definition

We provide the following five settings:

- 1) **Unsupervised IAD**. The training set only consists of m normal samples for each category.
- 2) **Semi-supervised IAD**. The training set consists of m normal samples and n abnormal samples, where $n \ll m$. The number of n could be 1, 2, 4, 5, 8, and 10 for the target category, respectively.
- 3) **Few-shot IAD**. Given a training set of only m normal samples, where $m \leq 8$, from a certain category. The number of m could be 1, 2, 4, and 8 for the target category, respectively.
- 4) **Noisy IAD**. Given a training set of m normal samples and n abnormal samples, n at most accounts for 20% of $m + n$. And n abnormal samples are labeled as normal samples for the training dataset.
- 5) **Continual IAD**. Given a finite sequence of training dataset consists of n categories, $\mathcal{T}_{train}^{total} = \{\mathcal{T}_{train}^1, \mathcal{T}_{train}^2, \dots, \mathcal{T}_{train}^n\}$, *i.e.*, $\mathcal{T}_{train}^{total} = \bigcup_{i=1}^n \mathcal{T}_{train}^i$, where the subsets \mathcal{T}_{train}^i consists of normal samples from one certain category $c_i, i \in n$. IAD algorithm is trained once for each category dataset \mathcal{T}_{train}^i in the CL scenario. At test time, the updated model are evaluated on each category of previous datasets, *i.e.*, $\mathcal{T}_{test}^{total} = \{\mathcal{T}_{test}^1, \mathcal{T}_{test}^2, \dots, \mathcal{T}_{test}^{i-1}\}$, respectively.

TABLE II
REPRESENTATIVE ALGORITHMS FOR IM-IAD. THE PURPLE ONES INDICATE OUR RE-IMPLEMENTATION METHODS.

Vanilla	Feature embedding	Normalizing flow	CS-Flow [56], FastFlow [78], CFlow [23], DifferNet [55]
		Memory bank	PaDiM [18], PatchCore [54], SPADE [12], CFA [35], SOMAD [38], [34]
		Teacher-student	RD4AD [21], STPM [67], [72], [5], [57]
		One-class classification	CutPaste [36], PANDA [51], DROC[62], MOCCA [45],PatchSVDD [76], SE-SVDD [28], [58]
	Reconstruction	External data usage	DREAM [79], DSR [81], MSTUnet[32], DFR [75]
		Without external data usage	FAVAE [19], NSA [59], RIAD [80], SCADN [73], InTra [49], [7], [27], [41], [13], [74], [20]
Semi-supervised		DRA [22], DevNet [48], FCDD [43], SPD [84], CAVGA [65], [11]	
Few-shot		RegAD [29], RFS [33],[61]	
Noisy		IGD [9], LOE [50], TrustMAE [64], SROC [14], SRR [77], CPCAD [16]	
Continual		DNE [39]	

B. Datasets

To perform comprehensive ablation studies, we employ 7 public datasets in the IM setting, including MVTec AD [4], [2], MVTec LOCO-AD [3] MPDD [31], BTAD [46], VisA [84], MTD [30], and DAGM [15]. Table III provides an overview of these datasets, including the number of samples (normal samples and abnormal samples), the number of classes, the types of anomalies, and the image resolution.

MVTec AD. The MVTec AD [4], [2] dataset is the most widely used dataset for industrial image anomaly detection. It contains 15 categories of items, including a training set consisting of 3,629 normal images, and a test set containing 467 normal and 1,258 abnormal images. The image resolution varies from 700×700 to 1024×1024 .

MVTec LOCO-AD. MVTec LOCO-AD [3] offers two types of anomalies, *i.e.*, structural anomalies and logical anomalies. There are 1,772 normal images in the training set and 304 normal images in the validation set. The test set consists of 575 normal images, 432 structurally abnormal images, and 561 logically abnormal images. Each image ranges from 850 to 1600 pixels in height and from 800 to 1700 pixels in width.

MPDD. There are six types of abnormal metal parts images in the MPDD dataset [31]. The authors of MPDD [31] capture each image with various angles, lightening conditions and distances. The training set consists of 888 normal images and the test set consists of 176 normal images and 282 abnormal images. The image resolution is 1024×1024 .

BTAD. BeanTech Anomaly Detection dataset (BTAD) [46] is a real-world dataset used for anomaly detection. The dataset contains 2,830 images of three industrial products with surface flaws.

VisA. VisA [84] is comprised of 9,621 normal samples and 1,200 abnormal samples. The image resolution varies from 960×960 to 1562×1562 . There are three major types of datasets in VisA. The first type of dataset is printed circuit boards (PCBs) with complex structures, which contains transistors, capacitors, and chips. The second type of dataset contains multiple instances in one view, which contains Capsules, Candles, Macaroni1 and Macaroni2. The term of multiple instances indicates that each image has multiple objects. The third type is single instances, which consists of Cashew, Chewing gum, Fryum and Pipe fryum. The anomaly types include scratches, dents, color sports, misplacement, and

missing parts.

MTD. Magnetic Tile Defects (MTD) [30] dataset consists of 1,344 images with the magnetic tile ROI clipped. There are six types of anomalies: blowhole, crack, fray, break, uneven and free (normal). To recreate the realism of an assembly line, the authors of MTD [30] photograph each item in several lightening conditions.

DAGM. DAGM [15] is a computer-generated surface-defect dataset. It contains grayscale images of ten different computer-generated surfaces and various defects, such as scratches or spots. There are 2,100 images for each type of anomalies.

TABLE III
COMPARISON OF DATASETS IN IM-IAD IN TERMS OF THE NUMBER OF NORMAL/ABNORMAL IMAGES, THE ANOMALY TYPES AND THE RESOLUTION OF IMAGES

Dataset	Samples		Classes		Sample Size	
	Normal	Anomaly	Anomaly Type	Object	Min	Max
MVTec AD	4,096	1,258	73	15	700	1,024
MVTec LOCO-AD	2,651	993	89	5	850	1,700
MPDD	1,064	282	5	1	1,024	1,024
BTAD	2,250	580	3	3	600	1,600
MTD	952	392	5	1	113	491
VisA	10,621	1,200	78	12	960	1,562
DAGM	15,000	2,100	10	10	512	512

C. Evaluation Metrics

In terms of structural anomalies, we employ Area Under the Receiver Operating Characteristics (AUROC/AUC), Area Under Precision Recall (AUPR/AP) and PRO [2] to evaluate the abilities of anomalies localization. Regarding logical anomalies, we adopt sPRO [6] to measure the ability of logical-defect detection. In addition, we use Forgetting Measure (FM) [8] to assess the ability of resisting catastrophic forgetting. In the following, we will give a detailed explanation of PRO, sPRO and FM.

Per-Region Overlap (PRO). Region-level metrics are more capable of assessing the ability of fine-grained anomaly detection. The ground truth is decomposed into its components. Let P_i represent the set of pixels predicted to be anomalous for a threshold τ , and let $C_{i,k}$ refer to the set of pixels flagged as anomalous for a connected component k in the i -th

ground truth picture. After that, the per-region overlap can be calculated as follows:

$$PRO = \frac{1}{N} \sum_i \sum_k \frac{|P_i \cap C_{i,k}|}{|C_{i,k}|}, \quad (1)$$

where N represents the test dataset's total number of ground truth components.

Saturated Per-Region Overlap (sPRO). sPRO is introduced by MVTEC LOCO-AD [6] and used to measure the logical and structural anomalies. Let $\{s_1, \dots, s_m\}$ denote a set of corresponding saturation thresholds such that $0 < s_i \leq |A_i|$ for all $i \in 1, \dots, m$ and $\{A_1, \dots, A_m\}$ refer to the set of all defect ground truth regions. For a set P of predicted abnormal pixels in the dataset, sPRO is defined as:

$$sPRO(P) = \frac{1}{m} \sum_{i=1}^m \min\left(\frac{|A_i \cap P|}{s_i}, 1\right), \quad (2)$$

The larger the sPRO value is, the better the performance of logical anomaly detection.

Forgetting Measure (FM) FM is defined as follows:

$$FM_j^k = \max_{l \in \{1, \dots, k-1\}} \mathbf{T}_{l,j} - \mathbf{T}_{k,j}, \quad (3)$$

where the number of tasks is k ; l is chosen in $[1, k-1]$; $T_{k,j}$ denotes that the model is trained from task 1 to task k and its performance is evaluated on task j ; $T_{l,j}$ denotes that the model is trained from task 1 to task l and its performance is evaluated on task j .

D. Baseline Methods

Table II lists 16 IAD algorithms (marked in purple) and their properties for IM-IAD. The criteria for selecting algorithms to be implemented for IM-IAD are that the algorithms should be representative in terms of supervision level (semi-supervised and unsupervised), noise-resilient capabilities, the facility of data-efficient adaptation (few-shot), and the capacity to overcome catastrophic forgetting. In addition, we classify unsupervised algorithms into two primary categories: feature-embedding-based and reconstruction-based methods. Since most of them achieve state-of-the-art performance on the majority of industrial image datasets, they are referred to as vanilla methods and compared in the IM setting.

Feature Embedding-based IAD. These methods are divided into four streams, *i.e.*, normalizing flow (FastFlow [78] and CSFlow [56]), memory bank (PatchCore [54], PaDiM [18], CFA [35] and SPADE [12]), teacher-student (RD4AD [21] and STPM [67]), and one-class classification (CutPaste [36]).

Reconstruction-based IAD. There are two typical algorithms for reconstruction-based methods. One is the reconstruction model that uses external data for training like DRAEM [79]; while the others do not use external data for training like FAVAE [19].

Semi-supervised IAD. As for exploring the benefits and drawbacks of semi-supervised anomaly detection methods, we select two state-of-the-art semi-supervised methods, *i.e.*, DRA [22] and DevNet [48]. Furthermore, we implement all unsupervised (vanilla) algorithms for few-shot experiments.

We intend to investigate the gap between semi-supervised IAD algorithms and vanilla unsupervised algorithms.

Few-shot IAD. RegAD [29] is chosen as the few-shot baseline method. In addition, we conduct few-shot ablation studies on the vanilla unsupervised IAD methods.

Noisy IAD. For comparison, we re-implement the cutting-edge noisy anomaly detection algorithm, IGD [9], and the vanilla unsupervised anomaly detection methods.

Continual IAD. Due to the paucity of research on continual IAD, we select only one method, DNE [39], to make a comparison with vanilla algorithms.

IV. RESULTS AND DISCUSSIONS

In this section, we analyze the existing algorithms in depth and discuss the important aspects under our proposed uniform IM setting. Note that, in each part, we describe the experimental settings, analyze the experimental results, and then outline the remaining challenges or future directions.

A. Overall Comparisons

Settings. A description of the compared vanilla methods is presented in Table II. The unsupervised setting is described in Sec. III-A-1. The details of the eight datasets are given in Sec. III-B.

Discussions. The statistical results from Table IV imply that there is no single winner on all datasets. In addition, Fig. 2(a) and Fig. 2(b) demonstrate that there is no dominating solution for accuracy, inference speed and GPU memory. Specifically, Table IV implies that PatchCore, one of the most cutting-edge memory bank-based methods, performs the best on the MVTEC AD dataset while performing the second-worst on the MVTEC LOCO-AD dataset. *Because the PatchCore architecture specializes in structural anomalies but not logical anomalies.* The primary distinction between MVTEC AD and MVTEC LOCO-AD is the types of anomalies.

Logical Anomalies Definition. MVTEC LOCO-AD is comprised of both structural anomalies and logical anomalies. Logical abnormalities are not dents or scratches, they are caused by dislocation or missing parts. But MVTEC AD only has a structural anomaly. Regarding the visualization results, Fig. 3 illustrates the limitation of each IAD model on various types of anomalies. For example, the images in the fifth column are screw bag and their defect types are logical anomalies. Specifically, each box of non-defect screw bag (the first row, the sixth column in Fig. 3) contains exactly *one pushpin*. But the defect screw bag (the second row, the sixth column in Fig. 3) contains two pushpins in the upper right corner box. The heatmap of PatchCore (the fourth row, the sixth column in Fig. 3) can not accurately depict the anomalies, *i.e.*, the right corner, while RD4AD [21] can precisely pinpoint the logical anomalies in the upper right corner.

Memory Usage and Inference Speed. It is evident from Fig. 2 that there is no dominating IAD method in terms of precision, memory usage and inference time. Though PatchCore achieves state-of-the-art performance in image AUC, it does not take advantage of memory usage and inference time.

TABLE IV

COMPARISON OF VANILLA IAD ALGORITHMS ON 7 DATASETS BY 5 METRICS (IMAGE AUC \uparrow , IMAGE AP \uparrow , PIXEL AUC \uparrow , PIXEL AP \uparrow AND PIXEL PRO \uparrow). THE BEST RESULT IS MARKED IN RED, AND THE NEXT BEST RESULT IS MARKED IN BLUE. WE REPORT sPRO WITH THE INTEGRATION PARAMETER OF 0.05.

Dataset	Metric	CFA	CS-Flow	CutPaste	DRAEM	FastFlow	FAVAE	PaDiM	PatchCore	RD4AD	SPADE	STPM
MVTec AD	Image AUC	0.981	0.952	0.918	0.981	0.905	0.793	0.908	0.992	0.986	0.854	0.924
	Image AP	0.993	0.975	0.965	0.990	0.945	0.913	0.954	0.998	0.995	0.940	0.957
	Pixel AUC	0.971	-	-	0.975	0.955	0.889	0.966	0.994	0.978	0.955	0.954
	Pixel AP	0.538	-	-	0.689	0.398	0.307	0.452	0.561	0.580	0.471	0.518
	Pixel PRO	0.898	-	-	0.921	0.856	0.749	0.913	0.943	0.939	0.895	0.879
MVTec LOCO-AD	Image AUC	0.814	0.814	0.734	0.798	0.639	0.623	0.780	0.835	0.867	0.687	0.679
	Image AP	0.944	0.942	0.915	0.933	0.866	0.873	0.927	0.948	0.958	0.890	0.891
	Pixel AUC	0.908	-	-	0.942	0.796	0.944	0.987	0.990	0.971	0.971	0.848
	Pixel AP	0.219	-	-	0.209	0.053	0.099	0.149	0.150	0.342	0.261	0.164
	Mean sPRO	0.581	-	-	0.426	0.357	0.446	0.521	0.343	0.637	0.520	0.428
MPDD	Image AUC	0.923	0.973	0.771	0.941	0.887	0.570	0.706	0.948	0.927	0.784	0.876
	Image AP	0.922	0.968	0.800	0.961	0.881	0.705	0.784	0.970	0.953	0.815	0.914
	Pixel AUC	0.948	-	-	0.918	0.808	0.906	0.955	0.990	0.987	0.982	0.981
	Pixel AP	0.283	-	-	0.288	0.115	0.088	0.155	0.432	0.455	0.342	0.354
	Pixel PRO	0.832	-	-	0.781	0.498	0.706	0.848	0.939	0.953	0.926	0.939
BTAD	Image AUC	0.938	0.936	0.917	0.895	0.919	0.923	0.965	0.947	0.937	0.904	0.918
	Image AP	0.980	0.890	0.953	0.974	0.867	0.986	0.976	0.989	0.985	0.974	0.962
	Pixel AUC	0.959	-	-	0.874	0.965	0.949	0.977	0.978	0.958	0.950	0.937
	Pixel AP	0.517	-	-	0.159	0.379	0.349	0.535	0.520	0.517	0.441	0.401
	Pixel PRO	0.702	-	-	0.629	0.725	0.713	0.798	0.752	0.723	0.745	0.667
MTD	Image AUC	0.913	0.887	0.830	0.782	0.891	0.795	0.885	0.975	0.884	0.868	0.729
	Image AP	0.959	0.945	0.912	0.885	0.947	0.867	0.944	0.988	0.947	0.928	0.847
	Pixel AUC	0.731	-	-	0.660	0.710	0.735	0.768	0.836	0.693	0.742	0.642
	Pixel AP	0.246	-	-	0.148	0.172	0.120	0.768	0.303	0.218	0.123	0.102
	Pixel PRO	0.528	-	-	0.541	0.568	0.632	0.798	0.686	0.623	0.627	0.478
VisA	Image AUC	0.920	0.744	0.819	0.887	0.822	0.803	0.891	0.951	0.960	0.821	0.833
	Image AP	0.935	0.787	0.848	0.905	0.843	0.843	0.895	0.962	0.965	0.847	0.873
	Pixel AUC	0.843	-	-	0.935	0.882	0.880	0.981	0.988	0.901	0.856	0.834
	Pixel AP	0.268	-	-	0.265	0.156	0.213	0.309	0.401	0.277	0.215	0.169
	Pixel PRO	0.551	-	-	0.724	0.598	0.679	0.859	0.912	0.709	0.659	0.620
DAGM	Image AUC	0.948	0.752	0.839	0.908	0.874	0.695	0.940	0.936	0.958	0.714	0.739
	Image AP	0.878	0.781	0.680	0.790	0.699	0.376	0.811	0.826	0.901	0.392	0.498
	Pixel AUC	0.942	-	-	0.868	0.911	0.804	0.961	0.967	0.975	0.880	0.859
	Pixel AP	0.495	-	-	0.306	0.342	0.170	0.492	0.517	0.534	0.133	0.151
	Pixel PRO	0.870	-	-	0.710	0.799	0.600	0.906	0.893	0.930	0.707	0.668

In practical industrial manufacturing scenarios, memory usage and inference speed must be fully considered. Hence, the present cutting-edge anomaly detection algorithm cannot meet the requirements of industrial manufacturing.

Pixel-Level or Image-Level Evaluation? It is urgent to set up a uniform assessment for the image-level and pixel-level of VAD performance. The majority of VAD metrics shrink the anomalous mask (ground truth) into the size of a feature map for evaluation, which inevitably reduces the precision of assessment. Moreover, according to Fig. IV, we discover that certain VAD methods, like PatchCore, perform well on image AUROC but poorly on pixel AP, or vice versa. Therefore, it is essential to develop a uniform metric for assessing VAD performance at both image and pixel levels.

Challenges. How to efficiently leverage visual anomaly types for unsupervised algorithm selection and design? Algorithm selection in accordance with anomaly types is crucial, despite the paucity of research in this area. Due to the low production line fault rate, collecting a significant number of anomalous samples for supervised training in industrial manufacturing is difficult. But since the product line specialist may provide information about anomalies type, being aware of

the type of visual anomalies beforehand is appropriate. In other words, for an unsupervised algorithm, knowledge of anomaly types can be considered as supervision information. Therefore, we recommend algorithm designers consider anomalous types while developing algorithms.

B. Role of Global Features in Logical IAD

Settings. We benchmark the vanilla unsupervised IAD algorithms on the MVTec LOCO-AD dataset. In addition, we also re-implement the baseline method of logical anomaly detection, GCAD [3].

Discussions. According to Table V, we find that the baseline method GCAD [3] is superior to all of unsupervised anomaly detection methods. The key idea of GCAD [3] is that it encodes feature descriptors of each pixel into global features via bottleneck architecture. Existing unsupervised IAD approaches have the disadvantage that their architectures are not optimized for global feature acquisition.

Challenges. Global feature extraction is essential for logical anomaly detection. The results in Table V indicate the importance of global anomaly feature extraction in achieving high detection performance for the logical IAD task.

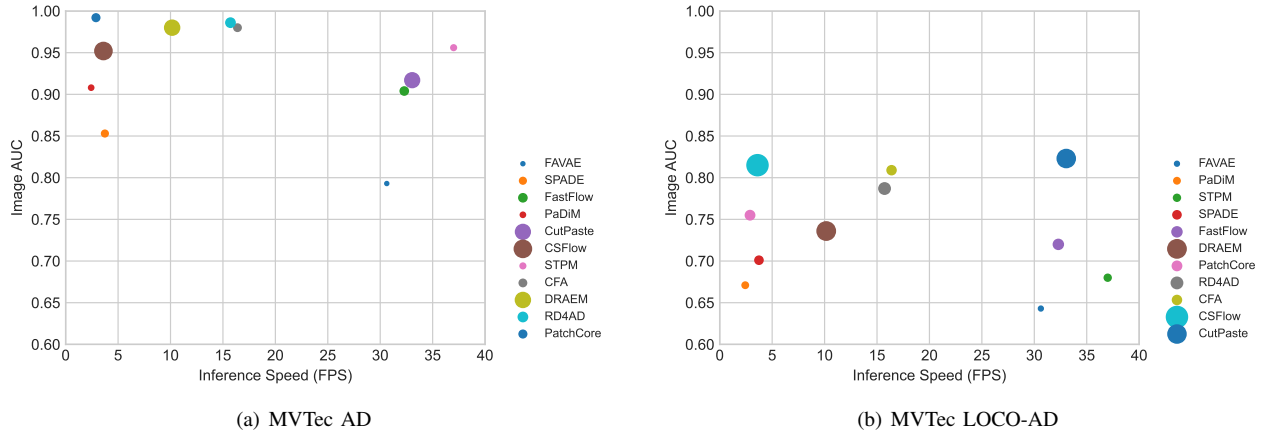


Fig. 2. Visualization of vanilla IAD algorithms on Image AUC ↑, inference time and GPU memory under MVTec AD and LOCO-AD. Y-axis denotes the performance of the IAD model. X-axis refers to the inference time for each image. The size of the circle denotes the GPU memory consumption of the IAD model during the test phase.

TABLE V

BENCHMARK ON MVTEC LOCO-AD DATASET IN TERMS OF LOGICAL ANOMALIES, STRUCTURAL ANOMALIES AND THEIR MEAN VALUE. THE BEST RESULT IS MARKED IN RED, THE NEXT BEST RESULT IS IN BLUE.

Method	Image AUROC ↑			Pixel sPRO ↑		
	Logical	Structural	Mean	Logical	Structural	Mean
PatchCore	0.690	0.820	0.755	0.340	0.345	0.343
CFA	0.768	0.851	0.809	0.536	0.625	0.581
SPADE	0.653	0.749	0.701	0.430	0.609	0.520
PaDiM	0.637	0.705	0.671	0.517	0.525	0.521
RD4AD	0.694	0.880	0.787	0.497	0.777	0.637
STPM	0.597	0.763	0.680	0.328	0.529	0.428
CutPaste	0.779	0.867	0.823	-	-	-
CSFlow	0.783	0.847	0.815	-	-	-
FastFlow	0.727	0.712	0.720	0.359	0.356	0.357
DRAEM	0.728	0.744	0.736	0.454	0.398	0.426
FAVAE	0.659	0.628	0.643	0.501	0.392	0.446
GCAD	0.860	0.806	0.833	0.711	0.692	0.701

To our knowledge, the latest network architectures, such as Transformer or Normalizing Flow, focus on long-distance feature extraction, which may make it simpler to spot logical anomalies. In particular, the statistical outcome of Table V demonstrates that CSFlow [56] based on the normalizing flow, achieves the second-best performance in terms of logical anomalies, indicating its tremendous potential. In addition, bottleneck architecture is another feasible approach to capturing global features. As shown in Fig. 3, the bottleneck design of RD4AD [21] is capable of obtaining the global feature, as shown by the heatmap of RD4AD on the logical-anomaly dataset.

C. Abnormal Data for Semi-supervised IAD

Settings. We first benchmark the basic unsupervised anomaly detection methods, and then assess semi-supervised methods with various numbers of anomalous training examples. In accordance with the definition of semi-supervised learning in Sec. III-A-2, we have set the number of anomaly samples for semi-supervised learning to 1, 2, 4, 5, 8, and 10, respectively. The training dataset for basic unsupervised

learning algorithms only contains normal samples for each category, but the training dataset for semi-supervised algorithms includes both normal and abnormal samples. “Method-N” denotes that the method utilizes N number of abnormal samples for training. For instance, DevNet-10 indicates that DevNet employs 10 abnormal samples for semi-supervised training.

TABLE VI

SEMI-SUPERVISED IAD VS UNSUPERVISED IAD ON BOTH IMAGE-LEVEL AND PIXEL-LEVEL METRICS. DEVNET-10 AND DRA-10 ARE SEMI-SUPERVISED METHODS USING 10 ANOMALY SAMPLES WITH ANNOTATIONS. THE OTHERS ARE UNSUPERVISED IAD METHODS. THE BEST RESULT IS MARKED IN RED, THE NEXT BEST RESULT IS IN BLUE.

Dataset	MVTec AD						MPDD						
	Image		Pixel		Pixel		Image		Pixel		Pixel		
Metric	AUC↑	AP↑	AUC↑	AP↑	PRO↑	AUC↑	AP↑	AUC↑	AP↑	PRO↑	AUC↑	AP↑	PRO↑
PatchCore	0.992	0.998	0.994	0.561	0.943	0.948	0.970	0.990	0.432	0.939	0.948	0.282	0.832
CFA	0.981	0.993	0.971	0.538	0.898	0.922	0.922	0.948	0.282	0.832	0.981	0.341	0.925
SPADE	0.854	0.940	0.955	0.470	0.894	0.784	0.815	0.981	0.341	0.925	0.981	0.341	0.925
PaDiM	0.908	0.954	0.966	0.452	0.913	0.705	0.784	0.955	0.155	0.848	0.955	0.155	0.848
RD4AD	0.986	0.994	0.978	0.579	0.939	0.927	0.952	0.986	0.455	0.953	0.927	0.952	0.986
STPM	0.895	0.953	0.954	0.518	0.879	0.876	0.913	0.981	0.354	0.939	0.876	0.913	0.939
CutPaste	0.917	0.965	-	-	-	0.771	0.800	-	-	-	0.771	0.800	-
CSFlow	0.952	0.975	-	-	-	0.972	0.967	-	-	-	0.972	0.967	-
FastFlow	0.905	0.944	0.955	0.398	0.855	0.886	0.881	0.808	0.114	0.497	0.886	0.881	0.808
DRAEM	0.981	0.989	0.974	0.688	0.921	0.940	0.960	0.917	0.288	0.781	0.940	0.960	0.917
FAVAE	0.793	0.913	0.888	0.306	0.749	0.570	0.705	0.906	0.088	0.705	0.570	0.705	0.906
DevNet-10	0.871	0.903	-	-	-	0.818	0.881	-	-	-	0.818	0.881	-
DRA-10	0.821	0.921	-	-	-	0.915	0.940	-	-	-	0.915	0.940	-

TABLE VII

SEMI-SUPERVISED IAD METHODS WITH RESPECT TO THE NUMBER OF ABNORMAL SAMPLES FOR TRAINING. THE BEST RESULT IS MARKED IN RED, THE NEXT BEST RESULT IS IN BLUE.

Dataset	Method	Metric	1	2	4	5	8	10
MVTec AD	DevNet	Image AUC	0.513	0.701	0.748	0.795	0.871	0.871
		Image AP	0.756	0.867	0.878	0.905	0.940	0.931
	DRA	Image AUC	0.603	0.682	0.749	0.763	0.794	0.822
		Image AP	0.813	0.859	0.891	0.891	0.908	0.922
MPDD	DevNet	Image AUC	0.508	0.582	0.774	0.822	0.850	0.818
		Image AP	0.597	0.672	0.816	0.870	0.890	0.882
	DRA	Image AUC	0.724	0.773	0.821	0.869	0.898	0.915
		Image AP	0.745	0.786	0.854	0.912	0.925	0.941

Discussions. Semi-supervised anomaly detection algorithms

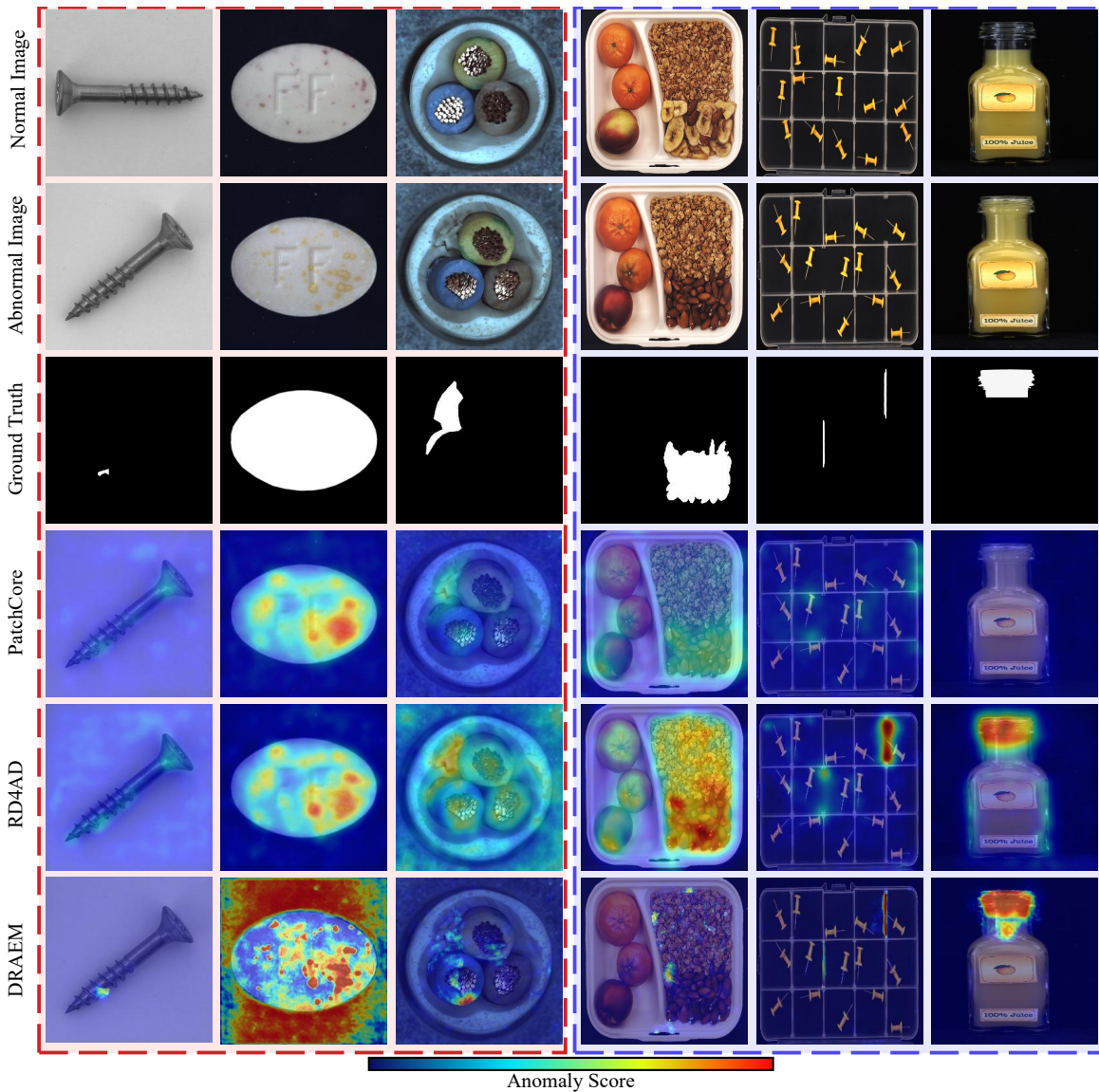


Fig. 3. Visualization of the representative vanilla IAD algorithms. The three columns on the left (marked in red) are structural anomalies, and the three columns on the right (marked in blue) are logical anomalies. The first row indicates the training images. In the vanilla IAD setting, all training images are normal. The second row denotes the test abnormal image. The third row shows the anomalies of the above abnormal image. The fourth, fifth and sixth row presents the heat map of PatchCore, RD4AD and DRAEM, respectively.

utilize the distance of feature space between test samples and training samples to predict the anomalies. The core idea behind semi-supervised anomaly detection is that the features of abnormal samples and normal samples are far from each other. But state-of-the-art few-shot methods are not good enough to depart the feature space of abnormal samples from the one of normal samples. For instance, DevNet [48] propose to use the deviation loss function to enforce a statistical deviation of the anomaly scores of all anomalies from those of normal samples. However, from Table VI, the performance of unsupervised IAD still surpass semi-supervised anomaly detection even if the number of labelled anomalies increases to 10. Moreover, Table VII reveals that DevNet-10 is worse than DevNet-8 on the MPDD dataset and DevNet-10 has the same performance as DevNet-8. In other words, adding additional anomalous data for training cannot improve the performance of semi-

supervised anomaly detection and may potentially degrade it. Thus, state-of-the-art few-shot IAD algorithms cannot take advantage of the information gained from labelled anomalies.

Challenges. It is necessary to re-design feature extraction algorithms and loss functions for the semi-supervised IAD setting. By observing the failure of semi-supervised IAD, we would call for more attention to the feature extraction and loss function, which can leverage both the guidance from labels efficiently and the exploration from the unlabeled data. Regarding the key problem mentioned above, improving feature extraction from abnormal samples and redesigning the deviation loss function can fully use labelled anomalies and diverge the feature space of abnormal samples from those of normal samples.

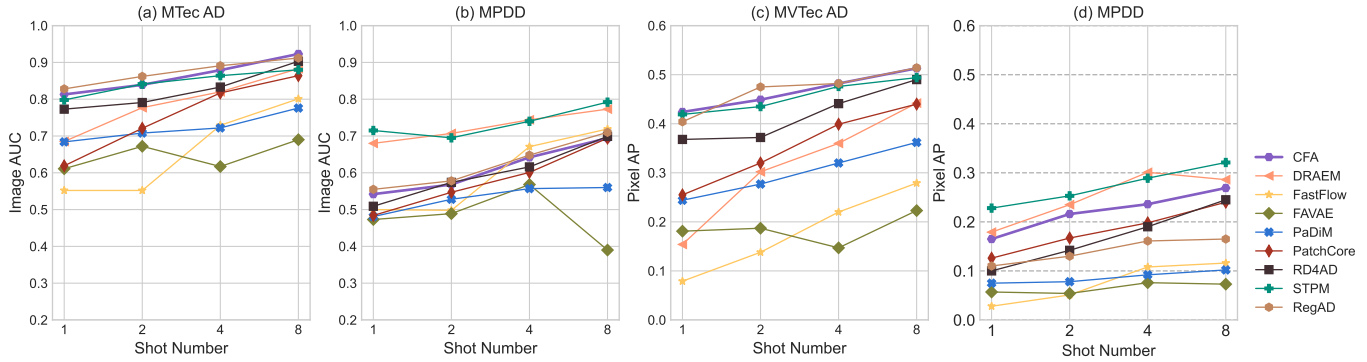


Fig. 4. Few-shot IAD Benchmark on MVTEC AD and MPDD. The Y-axis refers to metrics value and the X-axis denotes the shot number.

D. Rotation Augmentation for Feature-Embedding based Few-Shot IAD

Settings. With respect to the training samples, we choose 1, 2, 4, and 8 to benchmark vanilla IAD methods. The detail can be found in the few-shot setting of Sec. III-A-3. In addition, we make a comparison with RegAD [29], which is the advanced method in a meta-learning setting.

Discussions. Fig. 4 reveals that the performance of Cut-Paste, STPM and PatchCore are comparable to and even better than the baseline method, RegAD. Inspired by [47] and [10], we attempt to utilize data augmentation to improve their performance in the IM few-shot setting. The statistical result in Table VIII demonstrates that most data augmentation methods are sufficient for enhancing the performance of few-shot anomaly detection. In summary, we discover that rotation is the most efficient augmentation approach. Because we find out that most of datasets in realistic industrial images [4], [31] can be transformed to one another via rotation, such as the metal nut and the screw.

TABLE VIII

IMAGE AUC ↑ ON MVTEC AD WITH DATA AUGMENTATION, INCLUDING ROTATION, SCALE, TRANSLATION, FLIP, COLOR JITTER AND PERSPECTIVE. THE BEST RESULT IS MARKED IN RED, THE NEXT BEST RESULT IS IN BLUE. EACH DATA AUGMENTATION METHOD ENLARGES THE SAMPLE BY A FACTOR OF FOUR.

Method	Shot	Vanilla	Rotation	Scale	Translate	Flip	Color Jitter	Perspective
PatchCore	1	0.788	0.805	0.790	0.813	0.799	0.796	0.799
	2	0.795	0.831	0.801	0.810	0.822	0.800	0.802
	4	0.844	0.872	0.847	0.851	0.861	0.853	0.843
	8	0.891	0.916	0.888	0.896	0.907	0.885	0.890
CFA	1	0.813	0.811	0.788	0.789	0.837	0.816	0.762
	2	0.839	0.839	0.811	0.832	0.870	0.844	0.782
	4	0.879	0.879	0.821	0.876	0.890	0.888	0.792
	8	0.923	0.923	0.873	0.919	0.923	0.924	0.843

Challenges. Synthesizing abnormal samples is important yet difficult. Previously, we focused on developing a data augmentation method for normal images. However, we have not made much effort on synthesizing abnormal samples via data augmentation. In industrial manufacturing, it is very difficult to collect a large number of abnormal samples since most production lines are faultless. Hence, more attention should be paid to abnormal synthesis methods, like CutPaste [36], in the future.

E. Importance Re-weighting for Noisy IAD

Settings. Based on the noisy setting, which is introduced in Sec. III-A-4, we create a noisy-label training dataset by injecting various types of abnormal samples from the original test dataset. Specifically, we borrow the setting from Soft-Patch [71]. The abnormal samples mostly account for 20% (termed as noise ratio) of all training datasets. The noise ratio diverges from 5% to 20% and its step size is 5%. Due to the limited size of the test category, we select at most 75% abnormal samples of the test dataset for training. In the training phase, the observed labels of all training datasets are normal. In the test phase, the injection of abnormal samples is no longer evaluated. We benchmark the vanilla and noisy IAD baseline methods (IGD [9]) in IM noisy setting.

TABLE IX

IMAGE AUC ↑ OF NOISY IAD METHODS ON MVTEC AD AND MPDD UNDER VARIOUS NOISE RATIOS. THE BEST RESULT IS MARKED IN RED, THE NEXT BEST RESULT IS IN BLUE.

Dataset	MVTEC AD				MPDD			
	0.05	0.1	0.15	0.2	0.05	0.1	0.15	0.2
CFA	0.969	0.962	0.949	0.946	0.894	0.808	0.839	0.782
CS-Flow	0.939	0.894	0.904	0.874	0.773	0.789	0.861	0.727
CutPaste	0.864	0.900	0.851	0.907	0.773	0.671	0.653	0.683
DRAEM	0.954	0.912	0.869	0.897	0.810	0.760	0.726	0.693
FastFlow	0.885	0.867	0.854	0.855	0.836	0.725	0.725	0.691
FAVAE	0.768	0.801	0.798	0.814	0.536	0.476	0.482	0.525
IGD	0.805	0.801	0.782	0.790	0.797	0.786	0.789	0.756
PaDiM	0.890	0.907	0.899	0.906	0.675	0.580	0.626	0.608
PatchCore	0.990	0.986	0.975	0.980	0.857	0.790	0.782	0.763
RD4AD	0.989	0.984	0.975	0.983	0.909	0.837	0.826	0.824
SPADE	0.854	0.861	0.855	0.859	0.784	0.728	0.737	0.719
STPM	0.909	0.877	0.892	0.915	0.862	0.830	0.848	0.809

Discussions. According to the statistical result in Table IX, we discover feature embedding-based methods outperform IGD when the noise level is limited (≤ 0.15). To identify the cause, we deeply investigate one of the feature-embedding representative methods, PatchCore [54]. The architecture is depicted in detail in Fig. 5. The objective of the training phase is to construct a memory bank that stores the neighborhood-aware features from all normal samples. The feature memory construction method is shown in Algorithm 1.

By default, we set ResNet18 [26] as the feature extraction model. Coreset sampling [60] for memory bank aims to balance the size of memory bank with anomaly detection

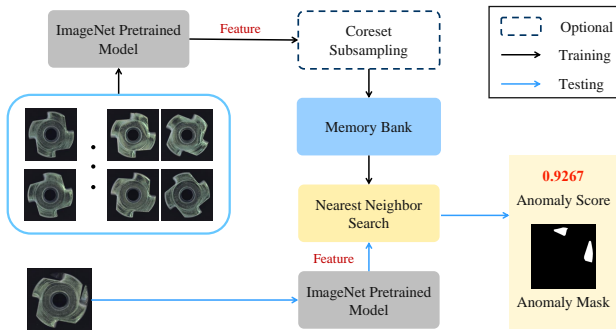


Fig. 5. Architecture of PatchCore. During training, nominal samples are split down into a memory bank of patch-level features that are neighborhood-aware. This memory bank is down-sampled by greedy coreset sub-sampling to minimize duplication and inference time. At the time of testing, images are identified as anomalies if at least one patch is abnormal, and pixel-level anomaly segmentation is obtained by scoring each patch-feature.

Algorithm 1: PatchCore Pipeline

Input : ImageNet pretrained ϕ , all normal samples \mathcal{X}_N
 patch feature extractor \mathcal{P} , memory size target l ,
 random linear projection ψ .

Output: Patch-level augmented memory bank \mathcal{M} .

```

1  $\mathcal{M} \leftarrow \{\}$ ;
2 for  $x_i \in \mathcal{X}_N$  do
3    $\mathcal{M} \leftarrow \mathcal{M} \cup \mathcal{P}(\phi(x_i))$ ;
4 end for
5  $\mathcal{M}_C \leftarrow \{\}$  //Apply coreset sampling for memory bank
6 for  $i \in [0, \dots, l-1]$  do
7    $m_i \leftarrow \arg \max_{m \in \mathcal{M} - \mathcal{M}_C} \min_{n \in \mathcal{M}_C} \|\psi(m) - \psi(n)\|_2$ ;
8    $\mathcal{M}_C \leftarrow \mathcal{M}_C \cup \{m_i\}$ ;
9 end for
10  $\mathcal{M} \leftarrow \mathcal{M}_C$ .
```

performance. During inference, the test image is predicted as anomalies if at least one patch is anomalous, and pixel-level anomaly segmentation is computed via the score of each patch feature. In particular, with the normal patches feature bank \mathcal{M} , the image-level anomaly score s for the test image x^{test} is computed by the maximum score s^* between the test image's patch feature $\mathcal{P}(x^{test})$ and its respective nearest neighbour m^* in \mathcal{M} :

$$m^* = \arg \max_{m^{test} \in \mathcal{P}(x^{test})} \arg \min_{m \in \mathcal{M}} \|m^{test} - m\|_2, \quad (4)$$

$$s^* = \|m^{test} - m^*\|_2. \quad (5)$$

To enhance the robustness of the anomaly detection model, PatchCore employs importance re-weighting method [40] to tune the anomaly score:

$$s = \left(1 - \frac{\exp \|m^{test,*} - m^*\|_2}{\sum_{m \in \mathcal{N}_b(m^*)} \exp \|m^{test,*} - m^*\|_2} \right) \cdot s^*, \quad (6)$$

where $\mathcal{N}_b(m^*)$ denotes b nearest patch-features in \mathcal{M} for test patch-feature m^* . Furthermore, we conduct the ablation study to verify the effect of re-weighting. The statistical result of Table X shows that re-weighting improves the resilience of IAD algorithms when the noise ratio is larger than 10%.

TABLE X
 IMAGE AUROC \uparrow OF PATCHCORE UNDER DIFFERENT NOISE RATIOS AND NEIGHBOURHOOD NUMBERS. THE BEST RESULT IS MARKED IN RED, THE NEXT BEST RESULT IS IN BLUE.

Noise Ratio	Neighbour Number				
	1 (No Re-weighting)	2	3	6	9
0.05	0.99	0.988	0.99	0.987	0.99
0.1	0.986	0.989	0.986	0.984	0.983
0.15	0.975	0.983	0.979	0.986	0.984
0.2	0.98	0.982	0.976	0.986	0.982

Challenges. Sample selection is crucial for improving the robustness of IAD. From Table IX, it is clear that the robust unsupervised IAD algorithms can be made better. We believe that sample selection has great potential for the future since it can be smoothly integrated with the current IAD methods. Establishing a specialized network to distinguish true-labeled instances from noisy training data is very popular [63], [44]. Two networks can be optimized in an end-to-end manner, *i.e.*, one is for sample selection and the other is for anomaly detection.

F. Memory Bank-based Methods for Continual IAD

Settings. We benchmark the vanilla methods and the continual baseline IAD method, DNE [39] according to the continual setting in Sec. III-A-5.

Discussions. Table XI shows that memory bank-based methods provide satisfying performance to overcome catastrophic forgetting phenomenon among all unsupervised IAD even though these methods are not specifically proposed for the continual IAD setting. The core idea behind that is that replay methods are perfectly fit for memory bank-based IAD algorithms. Memory bank-based methods can easily add new memory to alleviate forgetting while learning a new task. Thus, the memory bank ideally works for the rehearsal mechanism. During the test, memory bank-based methods are able to faultlessly combine the nearest-mean classifier to localize the nearest memory when given a test sample.

Challenges. In continual IAD settings, limiting memory bank size and minimizing interference from earlier tasks are of utmost significance. When learning a new task, just adding more memory will dramatically slow down the inference and increase storage usage. For a fixed storage need, we suggest using reservoir sampling [53] to set a limit on the number of instances that may be stored. In addition, the memory of a new task may overlap with the memory of the previous tasks, which might degrade IAD performance. Therefore, the primary challenge is to design a new constraint optimization loss function to avoid task interference.

G. Uniform View on IM-IAD

Settings. We benchmark all vanilla algorithms in our uniformed IM-IAD setting, including few-shot, noisy and continual setting. The details of the setting are described in Sec. III-A.

TABLE XI

PERFORMANCE AND CORRESPONDING FM ON THE CONTINUAL SETTING. THE BEST RESULT IS MARKED IN RED, THE NEXT BEST RESULT IS IN BLUE.

Dataset	MVTec AD					MPDD				
	Image		Pixel			Image		Pixel		
Method	AUC↑ / FM↓	AP↑ / FM↓	AUC↑ / FM↓	AP↑ / FM↓	PRO↑ / FM↓	AUC↑ / FM↓	AP↑ / FM↓	AUC↑ / FM↓	AP↑ / FM↓	PRO↑ / FM↓
PatchCore	0.919 / 0.003	0.971 / 0.001	0.944 / 0.002	0.481 / 0.005	0.847 / 0.001	0.786 / 0.015	0.851 / 0.021	0.963 / 0	0.358 / 0.0004	0.838 / 0.0001
CFA	0.623 / 0.361	0.813 / 0.181	0.753 / 0.217	0.176 / 0.359	0.535 / 0.363	0.506 / 0.415	0.609 / 0.307	0.818 / 0.131	0.116 / 0.164	0.557 / 0.300
SPADE	0.571 / 0.284	0.781 / 0.159	0.746 / 0.208	0.151 / 0.319	0.570 / 0.324	0.412 / 0.396	0.576 / 0.259	0.912 / 0.069	0.139 / 0.202	0.732 / 0.193
PaDiM	0.545 / 0.368	0.767 / 0.192	0.697 / 0.269	0.086 / 0.366	0.441 / 0.472	0.461 / 0.262	0.593 / 0.195	0.841 / 0.116	0.053 / 0.106	0.529 / 0.332
RD4AD	0.596 / 0.392	0.800 / 0.194	0.753 / 0.222	0.143 / 0.425	0.531 / 0.401	0.646 / 0.344	0.833 / 0.162	0.684 / 0.300	0.158 / 0.407	0.532 / 0.414
STPM	0.576 / 0.324	0.786 / 0.163	0.625 / 0.277	0.109 / 0.352	0.322 / 0.446	0.499 / 0.339	0.617 / 0.267	0.328 / 0.648	0.099 / 0.217	0.217 / 0.701
CutPaste	0.312 / 0.509	0.650 / 0.270	-	-	-	0.665 / 0.045	0.724 / 0.061	-	-	-
CSFlow	0.538 / 0.426	0.762 / 0.224	-	-	-	0.632 / 0.343	0.692 / 0.290	-	-	-
FastFlow	0.512 / 0.279	0.713 / 0.154	0.519 / 0.380	0.004 / 0.214	0.152 / 0.562	0.542 / 0.272	0.643 / 0.173	0.269 / 0.506	0.015 / 0.071	0.061 / 0.448
FAVAE	0.547 / 0.101	0.772 / 0.055	0.673 / 0.107	0.082 / 0.082	0.390 / 0.157	0.581 / 0.183	0.792 / 0.099	0.636 / 0.197	0.098 / 0.168	0.365 / 0.267
DNE	0.537 / 0.299	0.533 / 0.293	-	-	-	0.413 / 0.394	0.362 / 0.428	-	-	-

TABLE XII

BENCHMARK OF THE REPRESENTATIVE VANILLA IAD ALGORITHMS IN IM-IAD SETTING, INCLUDING FEW-SHOT, NOISY LABELING, CONTINUAL LEARNING. THE BEST RESULT IS MARKED IN RED, THE NEXT BEST RESULT IS IN BLUE.

Dataset	Metrics	Methods	MVTec AD				MPDD				
			Vanilla	Noisy-0.15	Few-shot-8	Continual	Mean	Vanilla	Noisy-0.15	Few-shot-8	Continual
Image AUC ↑	CFA	0.981	0.949	0.923	0.623	0.869	0.923	0.839	0.694	0.506	0.740
	CSFlow	0.952	0.904	0.845	0.539	0.810	0.973	0.861	0.741	0.633	0.802
	CutPaste	0.918	0.851	0.705	0.312	0.696	0.771	0.653	0.577	0.665	0.667
	DRAEM	0.981	0.869	0.883	0.595	0.832	0.941	0.726	0.773	0.440	0.720
	FastFlow	0.905	0.854	0.801	0.512	0.768	0.887	0.725	0.719	0.543	0.718
	FAVAE	0.793	0.798	0.690	0.547	0.707	0.570	0.482	0.390	0.582	0.506
	PaDiM	0.908	0.899	0.776	0.545	0.782	0.706	0.626	0.560	0.461	0.588
	PatchCore	0.992	0.975	0.864	0.919	0.938	0.948	0.782	0.694	0.787	0.803
	RD4AD	0.986	0.975	0.903	0.596	0.865	0.927	0.826	0.699	0.646	0.775
	SPADE	0.854	0.855	0.781	0.571	0.765	0.784	0.737	0.594	0.412	0.632
STPM	0.924	0.892	0.880	0.576	0.818	0.876	0.848	0.792	0.499	0.754	
Pixel AP ↑	CFA	0.538	0.394	0.513	0.177	0.406	0.283	0.212	0.269	0.117	0.220
	CSFlow	-	-	-	-	-	-	-	-	-	-
	CutPaste	-	-	-	-	-	-	-	-	-	-
	DRAEM	0.689	0.337	0.442	0.098	0.391	0.288	0.174	0.286	0.131	0.220
	FastFlow	0.398	0.313	0.279	0.044	0.259	0.115	0.055	0.116	0.015	0.075
	FAVAE	0.307	0.319	0.223	0.083	0.233	0.088	0.080	0.073	0.099	0.085
	PaDiM	0.452	0.454	0.362	0.086	0.339	0.155	0.136	0.102	0.053	0.112
	PatchCore	0.561	0.500	0.440	0.481	0.496	0.432	0.254	0.240	0.358	0.321
	RD4AD	0.580	0.532	0.490	0.143	0.436	0.455	0.374	0.245	0.158	0.308
	SPADE	0.471	0.410	0.405	0.151	0.359	0.342	0.309	0.261	0.140	0.263
STPM	0.518	0.465	0.494	0.110	0.354	0.354	0.309	0.321	0.100	0.271	

Discussions. It is evident from Table XII that PatchCore achieves the state-of-the-art result in our IM setting. However, as demonstrated in Fig. 2, PatchCore is inferior to other IAD algorithms in terms of GPU memory utilization and inference time, making their use in real production scenarios challenging. Furthermore, maintaining the size of the memory bank of PatchCore is a critical issue for realistic deployment if the number of object classes exceeds 100. Therefore, to bridge the gap between academic research and industrial manufacturing, there are still opportunities for IAD algorithms advancement.

Challenges. Multi-objective neural architecture search is a considerably promising approach. Given that test samples are sequentially streamed on the product line, most of IAD methods are incapable of making instantaneous predictions upon the arrival of a new test sample. Moreover, the memory capacity of edge devices used in practical manufacturing lines is restricted. Thus, regarding industrial manufacturing, IAD’s inference speed and memory usage should be addressed in addition to its accuracy. Adopting multi-objective evolutionary neural architecture search algorithms to find the optimal trade-off architecture is thus a promising approach.

V. CONCLUSION

We introduce IM-IAD in this paper, thus far the most complete industrial manufacturing-based image anomaly detection benchmark with 16 algorithms, 7 datasets, and 5 settings. We have gain insights into the importance of partial labels for semi-supervised learning, the influence of the neighborhood in noisy settings, the principles of creating architecture for continual learning, and logical anomalies based on assessments of numerous comparison angles. On top of these, we present several intriguing future lines of investigation for industrial image anomaly detection.

ACKNOWLEDGMENTS

This work is supported by the National Natural Science Foundation of China under Grant No. 61972188, 62122035, and 62206122.

REFERENCES

- [1] Anonymous. Pushing the limits of fewshot anomaly detection in industry vision: Graphcore. In *Submitted to The Eleventh International Conference on Learning Representations*, 2023. under review. 1, 2

- [2] Paul Bergmann, Kilian Batzner, Michael Fauser, David Sattlegger, and Carsten Steger. The mvtec anomaly detection dataset: a comprehensive real-world dataset for unsupervised anomaly detection. *International Journal of Computer Vision*, 129(4):1038–1059, 2021. **5**
- [3] Paul Bergmann, Kilian Batzner, Michael Fauser, David Sattlegger, and Carsten Steger. Beyond dents and scratches: Logical constraints in unsupervised anomaly detection and localization. *International Journal of Computer Vision*, 130(4):947–969, 2022. **5, 7**
- [4] Paul Bergmann, Michael Fauser, David Sattlegger, and Carsten Steger. Mvtec ad — a comprehensive real-world dataset for unsupervised anomaly detection. *2019 IEEE/CVF Conference on Computer Vision and Pattern Recognition (CVPR)*, pages 9584–9592, 2019. **5, 10**
- [5] Paul Bergmann, Michael Fauser, David Sattlegger, and Carsten Steger. Uninformed students: Student-teacher anomaly detection with discriminative latent embeddings. In *Proceedings of the IEEE/CVF Conference on Computer Vision and Pattern Recognition*, pages 4183–4192, 2020. **3, 5**
- [6] Paul Bergmann, Xin Jin, David Sattlegger, and Carsten Steger. The mvtec 3d-ad dataset for unsupervised 3d anomaly detection and localization. *arXiv preprint arXiv:2112.09045*, 2021. **5, 6**
- [7] Paul Bergmann, Sindy Löwe, Michael Fauser, David Sattlegger, and Carsten Steger. Improving unsupervised defect segmentation by applying structural similarity to autoencoders. *arXiv preprint arXiv:1807.02011*, 2018. **5**
- [8] Arslan Chaudhry, Puneet Kumar Dokania, Thalaiyasingam Ajanthan, and Philip H. S. Torr. Riemannian walk for incremental learning: Understanding forgetting and intransigence. *ArXiv*, abs/1801.10112, 2018. **5**
- [9] Yuanhong Chen, Yu Tian, Guansong Pang, and G. Carneiro. Deep one-class classification via interpolated gaussian descriptor. In *AAAI*, 2022. **4, 5, 6, 10**
- [10] Z. Chen, Yanwei Fu, Kaiyu Chen, and Yu-Gang Jiang. Image block augmentation for one-shot learning. In *AAAI Conference on Artificial Intelligence*, 2019. **10**
- [11] Wen-Hsuan Chu and Kris M Kitani. Neural batch sampling with reinforcement learning for semi-supervised anomaly detection. In *European conference on computer vision*, pages 751–766. Springer, 2020. **4, 5**
- [12] Niv Cohen and Yedid Hoshen. Sub-image anomaly detection with deep pyramid correspondences. *arXiv preprint arXiv:2005.02357*, 2020. **3, 4, 5, 6**
- [13] Anne-Sophie Collin and Christophe De Vleeschouwer. Improved anomaly detection by training an autoencoder with skip connections on images corrupted with stain-shaped noise. In *2020 25th International Conference on Pattern Recognition (ICPR)*, pages 7915–7922. IEEE, 2021. **5**
- [14] Antoine Cordier, Benjamin Missaoui, and Pierre Gutierrez. Data refinement for fully unsupervised visual inspection using pre-trained networks. *arXiv preprint arXiv:2202.12759*, 2022. **5**
- [15] German chapter of the IAPR (International Association for Pattern Recognition) DAGM (Deutsche Arbeitsgemeinschaft für Mustererkennung e.V. and the GNSS (German Chapter of the European Neural Network Society). Dagm dataset. <http://www.thisisurl/>, 2000. **5**
- [16] Puck de Haan and Sindy Löwe. Contrastive predictive coding for anomaly detection. *arXiv preprint arXiv:2107.07820*, 2021. **5**
- [17] Thomas Defard, Aleksandr Setkov, Angélique Loesch, and Romaric Audigier. Padim: a patch distribution modeling framework for anomaly detection and localization. In *ICPR Workshops*, 2020. **3**
- [18] Thomas Defard, Aleksandr Setkov, Angélique Loesch, and Romaric Audigier. Padim: a patch distribution modeling framework for anomaly detection and localization. In *International Conference on Pattern Recognition*, pages 475–489. Springer, 2021. **4, 5, 6**
- [19] David Dehaene and Pierre Eline. Anomaly localization by modeling perceptual features. *ArXiv*, abs/2008.05369, 2020. **4, 5, 6**
- [20] David Dehaene, Oriël Frigo, Sébastien Combreselle, and Pierre Eline. Iterative energy-based projection on a normal data manifold for anomaly localization. In *International Conference on Learning Representations*, 2019. **5**
- [21] Hanqiu Deng and Xingyu Li. Anomaly detection via reverse distillation from one-class embedding. *ArXiv*, abs/2201.10703, 2022. **5, 6, 8**
- [22] Choubo Ding, Guansong Pang, and Chunhua Shen. Catching both gray and black swans: Open-set supervised anomaly detection. In *Proceedings of the IEEE/CVF Conference on Computer Vision and Pattern Recognition*, pages 7388–7398, 2022. **1, 2, 5, 6**
- [23] Denis Gudovskiy, Shun Ishizaka, and Kazuki Kozuka. Cflow-ad: Real-time unsupervised anomaly detection with localization via conditional normalizing flows. In *Proceedings of the IEEE/CVF Winter Conference on Applications of Computer Vision*, pages 98–107, 2022. **3, 5**
- [24] Songqiao Han, Xiyang Hu, Hailiang Huang, Mingqi Jiang, and Yue Zhao. Adbench: Anomaly detection benchmark. *ArXiv*, abs/2206.09426, 2022. **1, 2**
- [25] Kaiming He, X. Zhang, Shaoqing Ren, and Jian Sun. Deep residual learning for image recognition. *2016 IEEE Conference on Computer Vision and Pattern Recognition (CVPR)*, pages 770–778, 2015. **3**
- [26] Kaiming He, X. Zhang, Shaoqing Ren, and Jian Sun. Identity mappings in deep residual networks. *ArXiv*, abs/1603.05027, 2016. **10**
- [27] Jinlei Hou, Yingying Zhang, Qiaoyong Zhong, Di Xie, Shiliang Pu, and Hong Zhou. Divide-and-assemble: Learning block-wise memory for unsupervised anomaly detection. In *Proceedings of the IEEE/CVF International Conference on Computer Vision*, pages 8791–8800, 2021. **5**
- [28] Chuanfei Hu, Kai Chen, and Hang Shao. A semantic-enhanced method based on deep svdd for pixel-wise anomaly detection. In *2021 IEEE International Conference on Multimedia and Expo (ICME)*, pages 1–6. IEEE, 2021. **3, 5**
- [29] Chaoqin Huang, Haoyan Guan, Aofan Jiang, Ya Zhang, Michael Spratling, and Yan-Feng Wang. Registration based few-shot anomaly detection. *arXiv preprint arXiv:2207.07361*, 2022. **4, 5, 6, 10**
- [30] Yibin Huang, Congying Qiu, and Kui Yuan. Surface defect saliency of magnetic tile. *The Visual Computer*, 36(1):85–96, 2020. **5**
- [31] Stepan Jezek, Martin Jonak, Radim Burget, Pavel Dvorak, and Milos Skotak. Deep learning-based defect detection of metal parts: evaluating current methods in complex conditions. In *2021 13th International Congress on Ultra Modern Telecommunications and Control Systems and Workshops (ICUMT)*, pages 66–71. IEEE, 2021. **5, 10**
- [32] Jielin Jiang, Jiale Zhu, Muhammad Bilal, Yan Cui, Neeraj Kumar, Ruihan Dou, Feng Su, and Xiaolong Xu. Masked swin transformer unet for industrial anomaly detection. *IEEE Transactions on Industrial Informatics*, 2022. **4, 5**
- [33] Ammar Mansoor Kamoona, Amirali Khodadadian Gostar, Alireza Bab-Hadiashar, and Reza Hoseinnezhad. Anomaly detection of defect using energy of point pattern features within random finite set framework. *arXiv preprint arXiv:2108.12159*, 2021. **4, 5**
- [34] Jin-Hwa Kim, Do-Hyeong Kim, Saehoon Yi, and Taehoon Lee. Semi-orthogonal embedding for efficient unsupervised anomaly segmentation. *arXiv preprint arXiv:2105.14737*, 2021. **3, 5**
- [35] Sungwook Lee, Seunghyun Lee, and Byung Cheol Song. Cfa: Coupled-hypersphere-based feature adaptation for target-oriented anomaly localization. *arXiv preprint arXiv:2206.04325*, 2022. **5, 6**
- [36] Chun-Liang Li, Kihyuk Sohn, Jinsung Yoon, and Tomas Pfister. Cut-paste: Self-supervised learning for anomaly detection and localization. In *Proceedings of the IEEE/CVF Conference on Computer Vision and Pattern Recognition*, pages 9664–9674, 2021. **5, 6, 10**
- [37] Lu Li, Wei Li, Qian Du, and Ran Tao. Low-rank and sparse decomposition with mixture of gaussian for hyperspectral anomaly detection. *IEEE Transactions on Cybernetics*, 51(9):4363–4372, 2020. **1**
- [38] Ning Li, Kaitao Jiang, Zhiheng Ma, Xing Wei, Xiaopeng Hong, and Yihong Gong. Anomaly detection via self-organizing map. In *2021 IEEE International Conference on Image Processing (ICIP)*, pages 974–978. IEEE, 2021. **3, 5**
- [39] Wujin Li, Jiawei Zhan, Jinbao Wang, Bizhong Xia, Bin-Bin Gao, Jun Liu, Chengjie Wang, and Feng Zheng. Towards continual adaptation in industrial anomaly detection. In *Proceedings of the 30th ACM International Conference on Multimedia*, pages 2871–2880, 2022. **1, 5, 6, 11**
- [40] Tongliang Liu and Dacheng Tao. Classification with noisy labels by importance reweighting. *IEEE Transactions on Pattern Analysis and Machine Intelligence*, 38:447–461, 2014. **11**
- [41] Wenqian Liu, Runze Li, Meng Zheng, Srikrishna Karanam, Ziyang Wu, Bir Bhanu, Richard J Radke, and Octavia Camps. Towards visually explaining variational autoencoders. In *Proceedings of the IEEE/CVF Conference on Computer Vision and Pattern Recognition*, pages 8642–8651, 2020. **5**
- [42] Ze Liu, Yutong Lin, Yue Cao, Han Hu, Yixuan Wei, Zheng Zhang, Stephen Lin, and Baining Guo. Swin transformer: Hierarchical vision transformer using shifted windows. *2021 IEEE/CVF International Conference on Computer Vision (ICCV)*, pages 9992–10002, 2021. **3**
- [43] Philipp Liznerski, Lukas Ruff, Robert A Vandermeulen, Billy Joe Franks, Marius Kloft, and Klaus Robert Müller. Explainable deep one-class classification. In *International Conference on Learning Representations*, 2020. **2, 5**
- [44] Yueming Lyu and Ivor Wai-Hung Tsang. Curriculum loss: Robust learning and generalization against label corruption. *ArXiv*, abs/1905.10045, 2019. **11**
- [45] Fabio Valerio Massoli, Fabrizio Falchi, Alperen Kantarci, Şeymanur Akti, Hazim Kemal Ekenel, and Giuseppe Amato. Mocca: Multilayer one-class classification for anomaly detection. *IEEE Transactions on Neural Networks and Learning Systems*, 2021. **3, 5**
- [46] Pankaj Mishra, Riccardo Verk, Daniele Fornasier, Claudio Piciarelli, and

- Gian Luca Foresti. Vt-adl: A vision transformer network for image anomaly detection and localization. In *2021 IEEE 30th International Symposium on Industrial Electronics (ISIE)*, pages 01–06. IEEE, 2021. [5](#)
- [47] Renkun Ni, Micah Goldblum, Amr Sharaf, Kezhi Kong, and Tom Goldstein. Data augmentation for meta-learning. In *International Conference on Machine Learning*, 2020. [10](#)
- [48] Guansong Pang, Choubo Ding, Chunhua Shen, and Anton van den Hengel. Explainable deep few-shot anomaly detection with deviation networks. *arXiv preprint arXiv:2108.00462*, 2021. [1](#), [4](#), [5](#), [6](#), [9](#)
- [49] Jonathan Pirnay and Keng Chai. Inpainting transformer for anomaly detection. In *International Conference on Image Analysis and Processing*, pages 394–406. Springer, 2022. [5](#)
- [50] Chen Qiu, Aodong Li, Marius Kloft, Maja Rudolph, and Stephan Mandt. Latent outlier exposure for anomaly detection with contaminated data. *arXiv preprint arXiv:2202.08088*, 2022. [4](#), [5](#)
- [51] Tal Reiss, Niv Cohen, Liron Bergman, and Yedid Hoshen. Panda: Adapting pretrained features for anomaly detection and segmentation. *2021 IEEE/CVF Conference on Computer Vision and Pattern Recognition (CVPR)*, pages 2805–2813, 2021. [5](#)
- [52] Danilo Jimenez Rezende and Shakir Mohamed. Variational inference with normalizing flows. In *International Conference on Machine Learning*, 2015. [3](#)
- [53] David Rolnick, Arun Ahuja, Jonathan Schwarz, Timothy P. Lillicrap, and Greg Wayne. Experience replay for continual learning. In *NeurIPS*, 2019. [11](#)
- [54] Karsten Roth, Latha Pemula, Joaquin Zepeda, Bernhard Schölkopf, Thomas Brox, and Peter Gehler. Towards total recall in industrial anomaly detection. In *Proceedings of the IEEE/CVF Conference on Computer Vision and Pattern Recognition*, pages 14318–14328, 2022. [4](#), [5](#), [6](#), [10](#)
- [55] Marco Rudolph, Bastian Wandt, and Bodo Rosenhahn. Same same but different: Semi-supervised defect detection with normalizing flows. In *Proceedings of the IEEE/CVF winter conference on applications of computer vision*, pages 1907–1916, 2021. [3](#), [5](#)
- [56] Marco Rudolph, Tom Wehrbein, Bodo Rosenhahn, and Bastian Wandt. Fully convolutional cross-scale-flows for image-based defect detection. In *Proceedings of the IEEE/CVF Winter Conference on Applications of Computer Vision*, pages 1088–1097, 2022. [3](#), [5](#), [6](#), [8](#)
- [57] Mohammadreza Salehi, Niousha Sadjadi, Soroosh Baselizadeh, Mohammad H Rohban, and Hamid R Rabiee. Multiresolution knowledge distillation for anomaly detection. In *Proceedings of the IEEE/CVF conference on computer vision and pattern recognition*, pages 14902–14912, 2021. [3](#), [5](#)
- [58] Daniel Sauter, Anna Schmitz, Fulya Dikici, Hermann Baumgartl, and Ricardo Bueftner. Defect detection of metal nuts applying convolutional neural networks. In *2021 IEEE 45th Annual Computers, Software, and Applications Conference (COMPSAC)*, pages 248–257. IEEE, 2021. [5](#)
- [59] Hannah M Schlüter, Jeremy Tan, Benjamin Hou, and Bernhard Kainz. Self-supervised out-of-distribution detection and localization with natural synthetic anomalies (nsa). *arXiv preprint arXiv:2109.15222*, 2021. [4](#), [5](#)
- [60] Ozan Sener and Silvio Savarese. Active learning for convolutional neural networks: A core-set approach. *arXiv: Machine Learning*, 2018. [10](#)
- [61] Shelly Sheynin, Sagie Benaim, and Lior Wolf. A hierarchical transformation-discriminating generative model for few shot anomaly detection. In *Proceedings of the IEEE/CVF International Conference on Computer Vision*, pages 8495–8504, 2021. [5](#)
- [62] Kihyuk Sohn, Chun-Liang Li, Jinsung Yoon, Minho Jin, and Tomas Pfister. Learning and evaluating representations for deep one-class classification. In *International Conference on Learning Representations*, 2020. [3](#), [5](#)
- [63] Hwanjun Song, Minseok Kim, and Jae-Gil Lee. Selfie: Refurbishing unclean samples for robust deep learning. In *International Conference on Machine Learning*, 2019. [11](#)
- [64] Daniel Stanley Tan, Yi-Chun Chen, Trista Pei-Chun Chen, and Wei-Chao Chen. Trustmae: A noise-resilient defect classification framework using memory-augmented auto-encoders with trust regions. In *Proceedings of the IEEE/CVF winter conference on applications of computer vision*, pages 276–285, 2021. [4](#), [5](#)
- [65] Shashanka Venkataramanan, Kuan-Chuan Peng, Rajat Vikram Singh, and Abhijit Mahalanobis. Attention guided anomaly localization in images. In *European Conference on Computer Vision*, pages 485–503. Springer, 2020. [4](#), [5](#)
- [66] Qian Wan, Liang Gao, and Xinyu Li. Logit inducing with abnormality capturing for semi-supervised image anomaly detection. *IEEE Transactions on Instrumentation and Measurement*, 71:1–12, 2022. [4](#)
- [67] Guodong Wang, Shumin Han, Errui Ding, and Di Huang. Student-teacher feature pyramid matching for anomaly detection. In *BMVC*, 2021. [3](#), [5](#), [6](#)
- [68] Hengli Wang, Rui Fan, Yuxiang Sun, and Ming Liu. Dynamic fusion module evolves drivable area and road anomaly detection: A benchmark and algorithms. *IEEE transactions on cybernetics*, 52(10):10750–10760, 2021. [1](#)
- [69] Minghua Wang, Qiang Wang, Danfeng Hong, Swalpa Kumar Roy, and Jocelyn Chanussot. Learning tensor low-rank representation for hyperspectral anomaly detection. *IEEE Transactions on Cybernetics*, 53(1):679–691, 2022. [1](#)
- [70] Jhih-Ciang Wu, Ding-Jie Chen, Chiou-Shann Fuh, and Tyng-Luh Liu. Learning unsupervised metaformer for anomaly detection. In *Proceedings of the IEEE/CVF International Conference on Computer Vision*, pages 4369–4378, 2021. [4](#)
- [71] Jiang Xi, Jianlin Liu, Jinbao Wang, Qiang Nie, WU Kai, Yong Liu, Chengjie Wang, and Feng Zheng. Softpatch: Unsupervised anomaly detection with noisy data. In *Advances in Neural Information Processing Systems*. [1](#), [2](#), [10](#)
- [72] Shinji Yamada and Kazuhiro Hotta. Reconstruction student with attention for student-teacher pyramid matching. *arXiv preprint arXiv:2111.15376*, 2021. [3](#), [5](#)
- [73] Xudong Yan, Huaidong Zhang, Xuemiao Xu, Xiaowei Hu, and Pheng-Ann Heng. Learning semantic context from normal samples for unsupervised anomaly detection. In *Proceedings of the AAAI Conference on Artificial Intelligence*, volume 35, pages 3110–3118, 2021. [5](#)
- [74] Yi Yan, Deming Wang, Guangliang Zhou, and Qijun Chen. Unsupervised anomaly segmentation via multilevel image reconstruction and adaptive attention-level transition. *IEEE Transactions on Instrumentation and Measurement*, 70:1–12, 2021. [5](#)
- [75] Jie Yang, Yong Shi, and Zhiquan Qi. Dfr: Deep feature reconstruction for unsupervised anomaly segmentation. *arXiv preprint arXiv:2012.07122*, 2020. [3](#), [5](#)
- [76] Jihun Yi and Sungroh Yoon. Patch svdd: Patch-level svdd for anomaly detection and segmentation. In *Proceedings of the Asian Conference on Computer Vision*, 2020. [3](#), [5](#)
- [77] Jinsung Yoon, Kihyuk Sohn, Chun-Liang Li, Sercan O Arik, Chen-Yu Lee, and Tomas Pfister. Self-supervise, refine, repeat: Improving unsupervised anomaly detection. 2021. [4](#), [5](#)
- [78] Jiawei Yu, Ye Zheng, Xiang Wang, Wei Li, Yushuang Wu, Rui Zhao, and Liwei Wu. Fastflow: Unsupervised anomaly detection and localization via 2d normalizing flows. *arXiv preprint arXiv:2111.07677*, 2021. [3](#), [5](#), [6](#)
- [79] Vitjan Zavrtanik, Matej Kristan, and Danijel Skočaj. Draem-a discriminatively trained reconstruction embedding for surface anomaly detection. In *Proceedings of the IEEE/CVF International Conference on Computer Vision*, pages 8330–8339, 2021. [3](#), [4](#), [5](#), [6](#)
- [80] Vitjan Zavrtanik, Matej Kristan, and Danijel Skočaj. Reconstruction by inpainting for visual anomaly detection. *Pattern Recognition*, 112:107706, 2021. [4](#), [5](#)
- [81] Vitjan Zavrtanik, Matej Kristan, and Danijel Skočaj. Dsr—a dual subspace re-projection network for surface anomaly detection. *arXiv preprint arXiv:2208.01521*, 2022. [4](#), [5](#)
- [82] Zheng Zhang and Xiaogang Deng. Anomaly detection using improved deep svdd model with data structure preservation. *Pattern Recognition Letters*, 148:1–6, 2021. [3](#)
- [83] Ye Zheng, Xiang Wang, Yu-Hang Qi, Wei Li, and Liwei Wu. Benchmarking unsupervised anomaly detection and localization. *ArXiv*, abs/2205.14852, 2022. [1](#), [2](#)
- [84] Yang Zou, Jongheon Jeong, Latha Pemula, Dongqing Zhang, and Onkar Dabeer. Spot-the-difference self-supervised pre-training for anomaly detection and segmentation. *arXiv preprint arXiv:2207.14315*, 2022. [5](#)